frontiers in Immunology

ORIGINAL RESEARCH
published: 10 September 2020
doi: 10.3389/fimmu.2020.01820

Galectin-3 in Prostate Cancer Stem-Like Cells Is Immunosuppressive and Drives Early Metastasis

Sara Caputo[1,2,3†], Matteo Grioni[1,2], Chiara S. Brambillasca[1,2†], Antonella Monno[4], Arianna Brevi[1,2], Massimo Freschi[2,5], Ignazio S. Piras[6], Angela R. Elia[1,2†], Valentina Pieri[7], Tania Baccega[3,8], Angelo Lombardo[3,8], Rossella Galli[7], Alberto Briganti[2,3,9], Claudio Doglioni[2,3,5], Elena Jachetti[1,2†] and Matteo Bellone[1,2]*

[1] Cellular Immunology Unit, Division of Immunology, Transplantation and Infectious Diseases, IRCCS San Raffaele Scientific Institute, Milan, Italy, [2] NET-IMPACT, IRCCS San Raffaele Scientific Institute, Milan, Italy, [3] Vita-Salute San Raffaele University, Milan, Italy, [4] Innate Immunity and Tissue Remodeling Unit, Division of Immunology, Transplantation and Infectious Diseases, IRCCS San Raffaele Scientific Institute, Milan, Italy, [5] Unit of Pathology, IRCCS San Raffaele Scientific Institute, Milan, Italy, [6] Neurogenomics Division, Center for Rare Childhood Disorders (C4RCD), Translational Genomics Research Institute, Phoenix, AZ, United States, [7] Neural Stem Cell Biology Unit, Division of Neuroscience, San Raffaele Scientific Institute, Milan, Italy, [8] San Raffaele Telethon Institute for Gene Therapy (SR-Tiget), IRCCS San Raffaele Scientific Institute, Milan, Italy, [9] Unit of Urology and URI, Division of Oncology, IRCCS Ospedale San Raffaele, Milan, Italy

Galectin-3 (Gal-3) is an extracellular matrix glycan-binding protein with several immunosuppressive and pro-tumor functions. The role of Galectin-3 in cancer stem-like cells (CSCs) is poorly investigated. Here, we show that prostate CSCs also colonizing prostate-draining lymph nodes of transgenic adenocarcinoma of the mouse prostate (TRAMP) mice overexpress Gal-3. Gal-3 contributes to prostate CSC-mediated immune suppression because either Gal-3 silencing in CSCs, or co-culture of CSCs and T cells in the presence of the Gal-3 inhibitor N-Acetyl-D-lactosamine rescued T cell proliferation. N-Acetyl-D-lactosamine also rescued the proliferation of T cells in prostate-draining lymph nodes of TRAMP mice affected by prostate intraepithelial neoplasia. Additionally, Gal-3 impacted prostate CSC tumorigenic and metastatic potential *in vivo*, as Gal-3 silencing in prostate CSCs reduced both primary tumor growth and secondary invasion. Gal-3 was also found expressed in more differentiated prostate cancer cells, but with different intracellular distribution as compared to CSCs, which suggests different functions of Gal-3 in the two cell populations. In fact, the prevalent nuclear and cytoplasmic distribution of Gal-3 in prostate CSCs made them less susceptible to apoptosis, when compared to more differentiated prostate cancer cells, in which Gal-3 was predominantly intra-cytoplasmic. Finally, we found Gal-3 expressed in human and mouse prostate intraepithelial neoplasia lesions and in metastatic lymph nodes. All together, these findings identify Gal-3 as a key molecule and a potential therapeutic target already in the early phases of prostate cancer progression and metastasis.

Keywords: prostate cancer, cancer stem cell, Galectin-3, immunosuppression, immune surveillance, prostate intraepithelial neoplasia, metastasis, T lymphocytes

OPEN ACCESS

Edited by:
Ira Ida Skvortsova, Innsbruck Medical University, Austria

Reviewed by:
Ying Ma, University of Texas MD Anderson Cancer Center, United States
Nahum Puebla-Osorio, University of Texas MD Anderson Cancer Center, United States

***Correspondence:**
Matteo Bellone
bellone.matteo@hsr.it

†Present address:
Sara Caputo, L-Nutra Italia SRL, Milan, Italy
Chiara S. Brambillasca, Department of Molecular Pathology, The Netherlands Cancer Institute, Amsterdam, Netherlands
Angela R. Elia, Institute of Oncology Research, Bellinzona, Switzerland
Elena Jachetti, Molecular Immunology Unit, Department of Research, Fondazione IRCCS Istituto Nazionale dei Tumori, Milan, Italy

Specialty section:
This article was submitted to Cancer Immunity and Immunotherapy, a section of the journal Frontiers in Immunology

Received: *05 March 2020*
Accepted: *07 July 2020*
Published: *10 September 2020*

Citation:
Caputo S, Grioni M, Brambillasca CS, Monno A, Brevi A, Freschi M, Piras IS, Elia AR, Pieri V, Baccega T, Lombardo A, Galli R, Briganti A, Doglioni C, Jachetti E and Bellone M (2020) Galectin-3 in Prostate Cancer Stem-Like Cells Is Immunosuppressive and Drives Early Metastasis. Front. Immunol. 11:1820. doi: 10.3389/fimmu.2020.01820

INTRODUCTION

Cancer is a multifactorial disease in which genetic and environmental factors concomitantly and progressively lead to neoplastic transformation and tumor development (1). According to the hierarchical model of cancer evolution, cancer stem-like cells (CSCs) represent the subpopulation of cancer cells within the tumor bulk that are endowed with tumorigenic potential, thus driving tumor growth and metastasis (2, 3). Nevertheless, cancer cells are not solitary entities, as they are embedded within the tumor microenvironment, which is composed of several players among which stromal cells (4), immune cells (5), and non-cellular components such as collagen fibers and glycosylated molecules, constituting the extracellular matrix (6, 7). A constant crosstalk between cancer cells and the tumor microenvironment ensures tumor development and progression.

Galectin-3 (Gal-3) is an extracellular matrix glycan-binding protein whose function spans several biological processes, including immune modulation, chemoattraction, cell adhesion, activation, differentiation, and apoptosis (8). Gal-3 is involved in several pathological events, and the function of Gal-3 depends on its location within the cell. When expressed on the plasma membrane or secreted, Gal-3 interacts with glycoconjugates, i.e., carbohydrate structures linked to lipids, proteins and peptides, thus mediating cell-cell, and cell-matrix interactions. In the cytoplasm, Gal-3 participates to the regulation of cell growth, cell cycle progression, and may inhibit apoptosis. Conversely, when localized into the nucleus, Gal-3 is pro-apoptotic. Given its pleiotropic effects, Gal-3 has been referred to as: "the guardian of the tumor microenvironment" (9).

Gal-3 is variably expressed in tumors, where it favors malignant transformation, invasion, and metastasis, and can also exert immunosuppressive functions (10, 11).

Gal-3 has been extensively investigated in prostate cancer (12). The healthy human prostate epithelium shows moderate immunostaining for Gal-3 that is localized both in the nucleus and the cytoplasm (13–16). In prostate intraepithelial neoplasia (PIN) lesions, Gal-3 expression is mainly cytoplasmic, more heterogeneous and more intense than in non-tumoral epithelium, but with a lower percentage of positive cells (14). Gal-3 expression is further reduced in prostate adenocarcinoma (13, 15), likely due to promoter methylation (17). Indeed, Gal-3 appears to be cleaved upon disease progression (18). However, in one report of 145 prostate cancer patients subjected to radical prostatectomy, the intensity of Gal-3 expression in carcinoma cells significantly associated with prostate specific antigen (PSA) relapse in univariate analysis, and exclusive cytoplasmic localization of Gal-3 was an independent prognostic indicator of biochemical progression after radical prostatectomy (14). Thus, localization within some cancer cells rather then percentage of tumor cells expressing Gal-3 seems relevant in prostate cancer. Additionally, Gal-3 favors prostate cancer metastasis, and oral administration of modified citrus pectin reduced the number of lung metastases in rats (19). Gal-3 has also been suggested as complementary diagnostic marker to PSA blood test, as serum concentration of Gal-3 was found increased in metastatic prostate cancer patients when compared to healthy subjects (20). Intriguingly, Gal-3 has also been proposed as potential biomarker at early clinical stages of prostate cancer (21).

Although little is known about Gal-3 function in CSCs, Gal-3 expression has been reported in CSCs from ovarian, gastrointestinal, kidney, and lung tumors (22–26). CSCs have been implicated in the development and progression of primary lesions and metastases (27). How precociously CSCs invade sites of prospective clinical metastasis still needs to be defined. Two general paradigms explain the process of systemic cancer progression (28). The linear progression model establishes that tumor ontogeny fully occurs in the primary tumor, and identifies metastasis as a late event that follows the development of a large tumor bulk. Consequently, metastases and primary tumor share genetic similarities. Conversely, the parallel progression model posits that tumor cells leave the primary lesion before acquisition of full malignant phenotype, and migrate to secondary sites where they acquire additional genetic hits. Thus, great genetic and epigenetic disparities characterize primary tumor cells and metastasis founders. We have previously reported that CSCs obtained from mouse PIN lesions [hereafter named as TPIN-SCs; ref. (29)], and concomitantly, from histopathology negative prostate draining lymph nodes were phenotypically and functionally identical, thus suggesting a common origin (30), and demonstrating that lymph node invasion may already occur at the early stage of PIN in transgenic adenocarcinoma of the mouse prostate (TRAMP) mice (31). Thus, our results support the hypothesis that prostate cancer adheres to the parallel progression model of metastasis.

Because Gal-3 is a key molecule involved in several aspects of tumor progression and metastasis (10), and our previous data suggested that TPIN-SCs over-express the Gal-3 transcript (29, 30), here we further investigated the expression of Gal-3 in TPIN-SCs, and asked if Gal-3 expressed by prostate CSCs plays a relevant role in the neoplastic process. Our findings demonstrate that already at the stage of mouse PIN, Gal-3 has a pivotal role in balancing tumorigenic, metastatic, and immunosuppressive abilities in CSCs.

MATERIALS AND METHODS

Mice

C57BL/6, C57BL/6-Tg(TcraTcrb)425Cbn/Crl, C57BL/6-Tg(TcraTcrb)1100Mjb/Crl (Charles River, Calco, Italy), and B6.129S7-Rag1tm1Mom/J mice (32) were housed in a pathogen-free animal facility. The latter two mouse strains were crossed to obtain RAG-$1^{-/-}$ OT1 mice. Heterozygous TRAMP mice (31) were generated as described (33). NOD.Cg-PrkdcscidIl2rgtm1Wjl/SzJ mice are also known as NOD scid gamma (NSG; Charles River, Calco, Italy). Animals were treated in accordance with the European Community guidelines and with the approval of the Institutional Ethical Committee.

Cell Culture

TPIN071122 and TNE070116 cells and the newly obtained TPIN1323 CSCs were cultured in NeuroCult™ NS-A Basal Medium (STEMCELL TECHNOLOGIES) supplemented with

heparin, EGF, and bFGF according to the manufacturing instructions, as described previously (29). Murine splenocytes were cultured in T cell medium (TCM), composed by RPMI (Lonza), with 10% fetal bovine serum (FBS; Invitrogen, Milan, Italy), 2 mM L-glutamine, 150 U/ml streptomycin and 200 U/ml penicillin (Cambrex, Milan, Italy), 10 mM Hepes, 10 mM Sodium Pyruvate and 5 μM β-mercaptoetanol (Gibco-Invitrogen, Milan, Italy). TRAMP-C2 cells (34) were cultured in DMEM (Lonza), with 10% FBS (Invitrogen). Unless specified, all chemical reagents were from Sigma-Aldrich (St. Louis, MO, USA). Peptides were kindly provided by R. Longhi (CNR, Milan, Italy). Human Du145 (35) and PC-3 cells (36) were cultured in RPMI (Lonza), with 10% FBS (Invitrogen).

Proliferation Assays

Splenocytes were labeled with the fluorescent dye carboxyfluorescein diacetate succinimidyl ester [CFSE, ref. (37)], and activated *in vitro* with anti-CD3 and anti-CD28 beads (Invitrogen) and IL-2 (R&D Systems, Minneapolis, MN, USA) according to the manufacturer instructions. When needed, irradiated (50 Gy) prostate CSC were added in co-culture at CSC:splenocyte ratio that corresponds to 1:10. When indicated, activated splenocytes were treated with 5 mM N-Acetyl-D-lactosamine (LacNac; Merck Life Science, Milan, Italy) 30 min before the addition of prostate CSCs. CFSE-labeled splenocytes from transgenic Rag-$1^{-/-}$ OTI mice were co-cultured with irradiated CSCs in the presence of the synthetic peptide $OVA_{257-264}$ (1 ng/ml) and 3.5 ng/ml IL-12 (R&D Systems) as previously described (38). After 4 or 3 days, respectively, cells were analyzed by FACS. Prostate-draining lymph nodes from TRAMP or WT mice were labeled with CFSE (30), cultured with or without 5 mM LacNAc, and analyzed after 3 days by FACS.

Gal-3 Silencing

TPIN071122 cells were stably infected with Gal-3 shRNA Lentiviral Particles or with control shRNA Lentiviral Particles (Sigma) at 10 MOI, according to the manifacturer's protocol, to generate TPIN-SCshGal3#5 and TPIN-SCshScram, respectively. Briefly, 5×10^4 cells/well were plated in a mixture of medium and Polybrene (Sigma). At day 2 lentiviral particles were added. At day 4 after infection, 2 μg/ml of puromycin dihydrochloride (Sigma) were added to select cells that had integrated the lentiviral particles.

Tumor Challenge

2×10^6 TPIN-SCshScram or TPIN-SCshGal3#5 were diluted 1:1 in Matrigel™ High Concentration (BD-Biosciences, Milan, Italy; 354248) and injected subcutaneously in male NSG recipients. 2×10^6 TRAMP-C2 cells were injected subcutaneously in male C57BL/6N recipients. Mice were monitored twice weekly. Mice were sacrificed if the tumor became ulcerated. Tumor size was evaluated by measuring two perpendicular diameters and height by a caliper. Because tumors grew homogeneously as ellipsoid shaped masses, their dimension was calculated applying the ellipsoid volume formula: $4/3\pi abc$, where a is height/2, b is width/2 and c is depth/2. To appreciate metastatic dissemination, the primary tumor was surgically resected when it achieved $\geq$ 80 mm^2 (major diameter × minor diameter) (39). Mice were sacrificed when lymph node metastases were palpable, and ∼1 month after surgery. Mice with no evidence of lymph node metastasis were killed 2 months after surgery.

Flow Cytometry

Single cell suspensions were obtained from cell cultures, incubated 10 min with FcR blocker (BD-Biosciences), labeled for 15 min at 4°C with fluorochrome-conjugated monoclonal antibodies or isotype controls (all from BD-Biosciences or BioLegend), and acquired by BD FACSCanto™ as previously described (40). Dead cells were excluded by gating on 7AAD staining or based on physical parameters. For apoptosis test, samples were stained in Annexin V binding buffer (BD). Data were analyzed using FlowJo software.

Western Blotting

Each cell pellet was homogenized in 10× volume of RIPA lysis buffer (10 mM Tris-Cl pH 7.2, 150 mM NaCl, 1 mM EDTA pH 8) with 1% Triton X-10/0.1% deoxycholate, 0.1% SDS, and protease and phosphatase inhibitor mixture (Roche). Samples were then diluted in Laemmli's SDS sample buffer. Proteins were separated by electrophoresis on 10% polyacrylamide gels according to the TGX Stain-Free FastCast Acrylamide kit protocol (Bio-Rad), and transferred onto Trans-Blot nitrocellulose membranes (Bio-Rad) according to the Trans-Blot Turbo Transfer System kit protocol (Bio-Rad). Ponceau staining (Sigma-Aldrich) was performed to confirm that the samples were loaded equally. The membranes were blocked in 5% non-fat dry milk in TBS-T (pH 7.4, with 0.1% Tween-20) for 1 h at room temperature. Primary antibodies were diluted in 3% BSA (Sigma-Aldrich) in TBS-T [mouse anti-calnexin 1:3,000 (Genetex) rat anti-mouse/human Gal-3 (E-Bioscience; 1:1,000)], and the membranes were incubated overnight at 4°C. The primary antibody was removed, and the blots were washed in TBS-T and then incubated for 45 min at room temperature in HRP-conjugated secondary antibodies [anti-mouse (Biorad) anti-rat (Amersham)]. Reactive proteins were visualized using a Clarity Western ECL substrate kit (Bio-Rad), and exposure was performed using UVItec (Cambridge MINI HD). Images were acquired by NineAlliance software.

Gal-3 Knocking Out

Gal3- and Cd44-KO cell lines were generated using CRISPR/Cas9 technology. sgRNA targeting the coding sequence of lagls3 (CTCAAGGATATCCGGGTGCA) or Cd44 (GATGTAACCTGCCGCTACGC) were cloned into a modified version of the lentiCRISPR lentiviral vector plasmid (Zhang lab, Addgene #52961). This third-generation lentiviral vector backbone was generated by replacing both the existing promoter with a Spleen Focus Forming Virus (SFFV) promoter (41) and the puromycin cassette with an enhanced Green Fluorescent Protein (eGFP) selection transgene, and by inserting a loxP site in the 3′-self-inactivating Long Terminal Repeat. A scramble sequence against the murine genome (GATCGGCAAGGTGTGGGTCG) was used as negative control. Vesicular stomatitis virus glycoprotein G pseudotyped lentiviral vectors stocks were prepared as previously described

(42). 10^5 TPIN1323 were brought at single-cell suspension and then transduced at multiplicity of infection of 5. Transduction medium was changed after 24 h and cells were expanded. Fifteen days after LV transduction, eGFP positive cells were sorted at BD FACSAria III (BD Bioscience), obtaining up to 98% cell purityImaging flow cytometry. Knock-out of Gal3 and Cd44 were evaluated by Surveyor Assay (41) and flow cytometry, respectively.

Imaging Flow Cytometry

The cells were resuspended at 40×10^6 cells/ml incubated 10 min with FcR blocker (BD-Biosciences), labeled for 30 min at 4°C with fluorochrome-conjugated monoclonal mouse/human Gal-3 antibodies (1:25; E-Bioscience) just before acquisition. For surface staining, fresh cells were also stained with 7AAD to exclude dead cells just before acquisition. For intracellular staining, cells were fixed with 2% PFA and permeabilized with Triton-X (0.1% in PBS), before incubation with the desired antibodies. Gal-3 antibody (1:100). Fresh samples were imaged by ImageStream IS100 Imaging Flow Cytometer (Amnis, Merck) using a 40× objective. The excitation laser powers used were as follow: 488 (150 mW) and 658 (90 mW). Fixed cells were instead imaged by ImageStream X MarkII Imaging Flow Cytometer using a 40× objective. The excitation laser powers used were as follow: 405 (10 mW), 488 (200 mW), and 642 (20 mW). At least 10,000 events were collected in each sample, and single stained controls were acquired with identical laser settings to create compensation matrix. Data analysis was performed using the IDEAS software (Amnis). First of all, cells were gated for cells in focus using the gradient root mean square feature and then single cells were identified using area and aspect ratio features on the brightfield image. In fixed samples we evaluated the intracellular localization of Gal-3 protein. Single cells were gated for Dapi and Gal-3 double positivity, and nuclear localization of Gal-3 was assessed by Similarity feature in the nuclear region. Similarity feature is the log transformed Pearson's Correlation Coefficient and is a measure of the degree to which two images are linearly correlated within a masked region (IDEAS software). Thus, when the intensity of Gal-3 in the nuclear region is high and Dapi staining is high, there is a linear correlation between the two images and the similarity feature has a high positive value.

Real-Time PCR

Total RNA from CSCs was extracted using the RNeasy Plus Mini kit (Qiagen, Chatsworth, CA, USA). cDNA was obtained from 1,000 ng of RNA using the M-MLV-Reverse Transcriptase kit (Promega, Madison, WI, USA). Real-Time PCR was performed in a total volume of 20 μL using the Taqman® Universal PCR Master Mix (Applied Biosystems, Monza, Italy), 2 μL of cDNA (prediluted 1:1) and specific probes for Gal-3 or L-19 (Applied Biosystems, Italy). Values were normalized to internal control (L-19) using the ΔCT method.

Immunohistochemistry and Immunofluorescence of Human and Mouse Samples

After institutional review board approval, a cohort of nine patients with pelvic node-positive prostate cancer treated with radical prostatectomy and extended pelvic lymph node dissection were randomly selected from our prospectively collected data-base. Human and TRAMP prostate or lymph node specimens were embedded in paraffin. Five micrometer sections were stained with Mayer- Hematoxylin and Eosin (BioOptica, Milan, Italy) and evaluated by an expert pathologist (33). Alternatively, after re-hydratation, antigen retrieval in 10 mM citric acid and blocking with 5% NGS, slides were incubated with the anti mouse/human Gal-3 (1:200; E-Bioscience) overnight at 4°C. A biotinylated secondary antibody was used 1:250 for 1 h at room temperature. Colorimetric revelation was made with Novared chromogen (Vector Labs, Burlingame, CA, USA). Slides were finally contrasted with Mayer-Hematoxylin (BioOptica), mounted with cover glass and examined under microscope (Carl Zeiss, Axioscope 40FL, Varese, Italy). Prostate CSCs or prostate cancer cells were plated on a matrigel-coated glass slide overnight, fixed with 4% PFA and permeabilized with PBS containing 0.1% Triton-X. After blocking with Triton X-100 0.1 and 5% NGS for 1 h at room temperature, cells were incubated with rat anti-mouse/human Gal-3 (E-Bioscience; 1:200) for 2 h at room temperature, and then with anti-rat Alexa 546 secondary antibody (E-bioscience; 1:200). Nuclei were stained with 0.1 μg/mL DAPI and slides were examined under TCS SP2 confocal microscope (Leica, Milan, Italy). For Oct-4 staining prostate CSCs were plated on a matrigel-coated glass slide overnight, fixed with 4% PFA and permeabilized with PBS containing 0.1% Triton-X and 2% BSA. After blocking with Triton X-100 0.1 and 5% NGS for 1 h at room temperature, cells were incubated with rat anti-mouse/human Oct-3/4 (Santa Cruz Biotechnology; 1:20) and rabbit anti-GFP (Invitrogen; 1:250) for 2 h at room temperature, and then with PE anti-mouse secondary antibody (Santa Cruz Biotechnology; 1:200) and anti-rabbit Alexa 488 secondary antibody (Life Technologies; 1:500), respectively. Nuclei were stained with 0.1 μg/mL DAPI and slides were examined under TCS SP2 confocal microscope (Leica, Milan, Italy).

IncuCyte

Cell and spheroid proliferations were assessed using Incucyte (Sartorius Essen Biosciences, AnnArbor, MI) over 88 h in culture, with image capture every 4 h. Cell and spheroid proliferations were measured and reported as mean area confluence percentage, IncuCyte Image Analysis Software. Spheroids identification was allowed by setting a minimum dimension in order to distinguish them from single cells.

Microarray-Based Gene Expression Profiling

Total RNA extracted using the RNeasy Micro and Mini kit (Qiagen, Chatsworth, CA, USA) was analyzed with Affimetrix Mouse Gene 1.0 ST Array as previously described (29).

Statistical Analyses

Statistical analyses were performed using the Student's *T*, One-Way Anova followed by Tukey's tests, or Fisher exact test. Values were considered statically significant for $^{*}p < 0.05$, $^{**}p < 0.01$; $^{***}p < 0.001$, $^{****}p < 0.0001$.

RESULTS

Gal-3 Favors Proliferation, Spheroid Formation, Tumorigenicity, and Metastatic Potential of TPIN-SCs

We have previously reported that TPIN-SCs, despite their highly metastatic behavior (43), can be targeted both by innate and adaptive immune cells (44), but are also endowed with immunosuppressive activities (45). In particular, we have found that TPIN-SCs use the extracellular matrix protein Tenascin-C to dampen T cell activation (30, 46), a mechanism that might favor their metastatic propensity. However, Tenascin-C silencing in TPIN-SC did not completely abolish their immunosuppressive activity, thus suggesting that additional molecules were involved in CSCs-mediated immunosuppression (30). In search for additional mechanisms favoring CSC aggressiveness, we mined data from transcriptomic analyses of TPIN-SCs and CSCs derived from neuroendocrine tumors (TNE-SCs; **Figure 1A**) (29, 30), the latter being devoid of immunosuppressive activity (30). We found that lgals3, the gene coding for Gal-3, was over-expressed in TPIN-SCs (**Figure 1B**). Gal-3 expression in TPIN-SCs was confirmed by real time PCR (**Figure 1C**), flow cytometry (**Figure 1D**), and western blot (**Figure 1E**).

To assess the role of Gal-3 in CSC biology, we infected TPIN-SCs with lentiviral vectors encoding either a Gal-3-specific or a scrambled short hairpin RNA (shGal-3#5 and shScram, respectively). qPCR, flow cytometry and western blot analyses (**Figures 1C–E**) confirmed Gal-3 silencing in prostate CSCs. Strikingly, Gal-3 silencing in TPIN-SCs reduced cell confluence (**Figures 2A,B**) and spheroid confluence and area (**Figures 2A,D,F**). These results, although consistent with the hypothesis that Gal-3 regulates proliferation and sphere formation in CSCs, were not conclusive because Gal-3 expression in TPIN-SCshGal-3#5 cells was not totally abolished (**Figure 1**). Thus, we generated TPIN-SCkoGal-3 cells by knocking out lgals3 in TPIN-SCs (**Supplementary Figure 1**), and we compared their proliferation and sphere formation capacity with TPIN-SCkoScram (**Supplementary Figure 1**). As shown in **Figure 2C**, TPIN-SCkoGal-3 proliferated less than TPIN-SCkoScram, thus confirming that Gal-3 is important for TPIN-SC proliferation. At difference with TPIN-SCshGal-3#5 cells, TPIN-SCkoGal-3 did not show a reduced spheroid confluence and area (**Figures 2E,G**). Indeed, spheroid confluence was higher in TPIN-SCkoGal-3 than in TPIN-SCkoScram. A direct comparison between TPIN-SCshGal-3#5 and TPIN-SCkoGal-3 cannot be done because they have been derived from two different CSCs lines. Nevertheless, data reported in **Figure 2** suggest that Gal-3 dynamically regulate both cell proliferation and cell adhesion. Indeed Gal-3 contributes to cell-cell and cell-matrix interactions (8). Thus, it can be hypothesized that in the absence of endogenous Gal-3, less proliferating CSCs remain in clusters. CSCs might also compensate lack of Gal-3 by upregulating expression of other molecules involved in spheroid formation.

To investigate the tumorigenic and metastatic potential of prostate CSCs in a context devoid of the potentially confounding effects of the immune system, immunodeficient NSG mice were challenged with TPIN-SCs either silenced or not for Gal-3. TPIN-SCshScram and TPIN-SCshGal-3#5 generated tumors in 100% of NSG mice, but tumor growth was delayed in mice challenged with TPIN-SCshGal-3#5 (**Figure 3A**), and at day 44, the tumor dimension was reduced in mice challenged with TPIN-SCshGal-3#5 when compared to mice challenged with TPIN-SCshScram (**Figure 3B**). These data demonstrate that Gal-3 has a relevant tumor-cell intrinsic effect on prostate cancer progression.

To investigate the metastatic potential of TPIN-SCs, the primary subcutaneous lesion was surgically resected when the tumor mass reached an area of $\geq$80 mm^2, and mice were monitored thereafter for metastasis occurrence. The primary lesion was excised to allow metastases to show up before mice had to be culled due to primary lesion overgrowth. Gal-3 silencing in TPIN-SCs reduced their metastatic potential. Indeed, metastases were found in 56% of the mice injected with TPIN-SCshScram, and only in 36% of TPIN-SCshGal-3#5-challenged mice (**Figure 3C**). Tumor-draining lymph nodes were the preferred site of invasion upon subcutaneous injection. Interestingly, Gal-3 silencing in TPIN-SCs significantly reduced their tropism for lymph node invasion, and metastatic lymph nodes were found in 24% of the mice injected with TPIN-SCshGal-3#5, and 50% of mice challenged with TPIN-SCshScram (**Figure 3D**). Lack of Gal-3 did not significantly impact metastatic appearance in the lungs (**Figure 3E**), kidneys (**Figure 3F**), and liver (**Figure 3G**). Altogether, these findings suggest that Gal-3 has a relevant tumorigenic and metastatic role in prostate CSCs.

Localization of Gal-3 in Prostate CSCs and in TRAMP-C2 Prostate Cancer Cells

Because subcellular Gal-3 localization correlates with its function in tumor cells (10), we analyzed prostate CSCs by flow cytometry, immunofluorescence, and imageStream technology, which combines flow cytometry with the detail imagery of microscopy. TPIN-SCs expressed Gal-3 at the cell surface (**Figure 4A**) and in the intracellular space (**Figures 4B,C**). Approximately 50% of the TPIN-SCs were Gal-3 positive both in the cytoplasm and in the nucleus, whereas the remaining 50% showed a preferential cytoplasmic localization (**Figures 4C,D**). Also TRAMP-C2 cells, a line of more differentiated prostate cancer cells obtained from a TRAMP adenocarcinoma (34), expressed Gal-3 (**Figures 4A–C**). However, the majority of TRAMP-C2 cells showed a preferential cytoplasmic localization of Gal-3 (**Figures 4B–D**). Thus, Gal-3 is differently distributed in TPIN-SCs and more differentiated prostate cancer cells.

It has been recently reported that Gal-3 promotes lung cancer stemness via the EGFR/c-Myc/Sox-2 pathway (24), and Oct4, a stemness-related transcription factor (47), favors Gal-3 expression, thus establishing a positive regulatory loop in lung CSCs (24). To investigate whether a different intracellular expression of Gal-3 associates with different functional states (i.e., stem cells and their differentiated progeny), we transduced prostaspheres generated from TPIN-SCs, which contained both CSCs and committed more differentiated precursors, with a lentiviral vector carrying the GFP sequence under the control

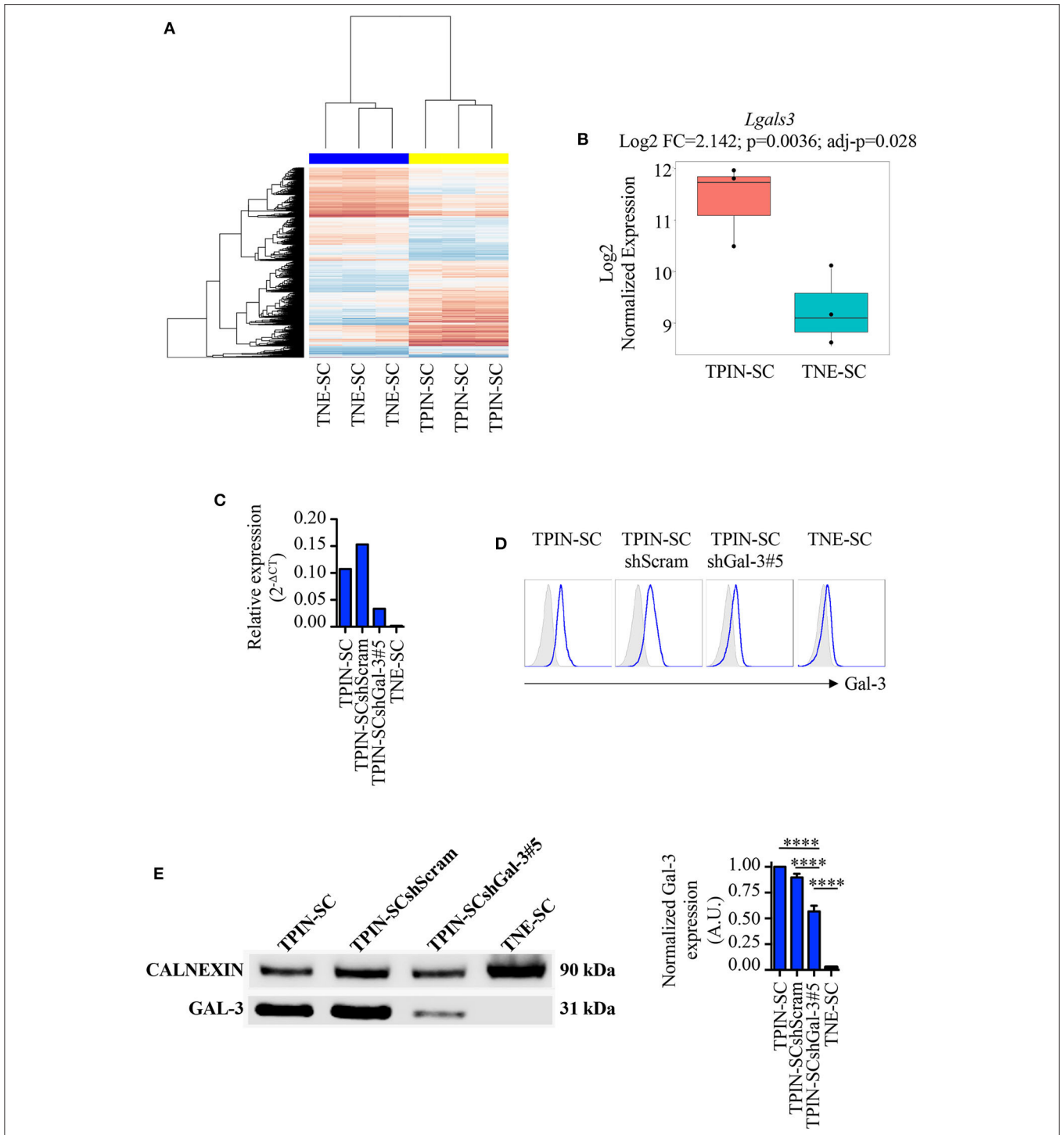

FIGURE 1 | Gal-3 is overexpressed in TPIN-SCs, and can be silenced by shRNA technology. Gene expression analysis of CSCs with Affimetrix Mouse Gene 1.0 ST Array. **(A)** Heatmap reports the global gene expression data in TPIN-SCs vs. TNE-SCs. Differentially expressed genes with a $p < 0.05$ are red (upregulated) or blue-colored (downregulated). **(B)** Boxplot reports Lgals3 expression in TPIN-SCs vs. TNE-SCs (Log2 FC = 2.142, $p = 0.0036$, *adj-p* = 0.028). Gal-3 silencing in TPIN-SCs was attempted with five different shRNA sequences. We obtained substantial inhibition of Gal-3 expression in all TPIN-SCs infected with viruses encoding Gal-3 specific shRNA (not shown). We selected TPIN-SCshGal-3#5 for our experiments. Expression of Gal-3 in the indicated cells was assessed by real-time PCR **(C)**, flow cytometry **(D)** and Western blot **(E)** analysis. **(C)** Relative expression of Gal-3 in the indicated cells was assessed by real-time PCR. **(D)** Fresh samples for cell surface detection of Gal-3 were stained with anti-Gal-3 antibody and 7AAD. The plots report representative histograms of Gal-3 staining (blue lines), gray histograms: isotype control. TNE-SCs were used as negative control for Gal-3 expression. The panel is representative of at least three independent experiments. **(E)** Western blotting analysis of total Gal-3 expression in the indicated cell lines and relative quantification. The Western blot is representative of two independent experiments, performed each time on biological duplicates. The graph is a pool of four independent blots. Statistical analysis was performed using the Anova Test. ****$p < 0.0001$.

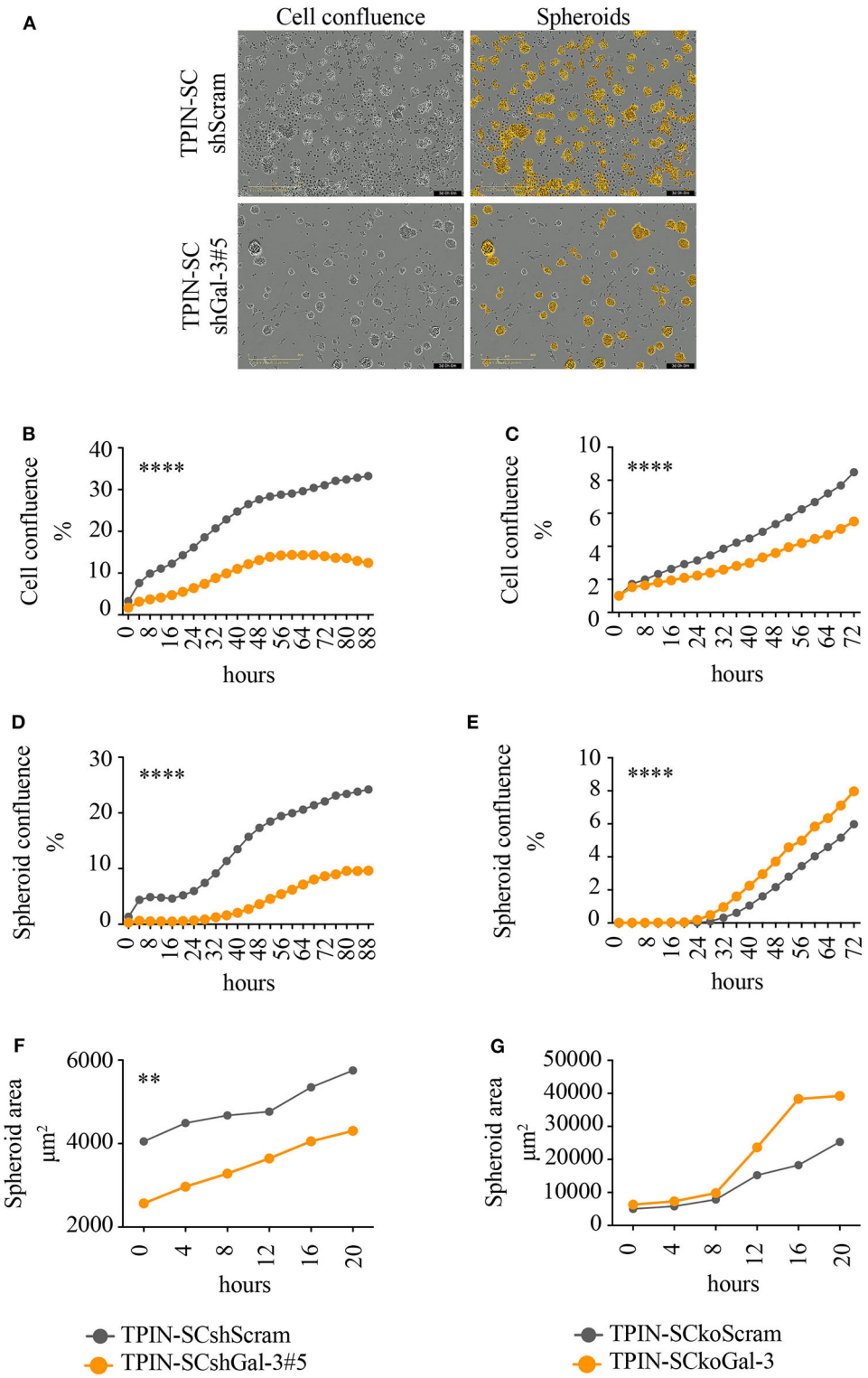

FIGURE 2 | Gal-3 impacts TPIN-SC proliferation, and sphere formation, tumorigenicity, and metastatic potential. TPIN-SCshScram or TPIN-SCshGal-3#5 were analyzed by IncuCyte for 88 h consecutively **(A,B,D,F)**, and TPIN-SCkoGal-3 and TPIN-SCkoScram were analyzed 72 h consecutively **(C,E,G)**, with image captured every 4 h. **(A)** Representative images of cell confluence and spheroids at day 3. Orange: mask to identify spheroids; objective: 10×; scale: 400 µm. **(B,C)** Cell proliferation was measured and reported as mean cell confluence percentage. **(D,E)** Spheroid proliferation was measured and reported as mean spheroid confluence percentage. **(F,G)** Spheroids dimension at day 3 was measured and reported as mean spheroid area (μm^2). Statistical analyses were performed using the Student *T*-test. $^{**}p < 0.01$; $^{****}p < 0.0001$.

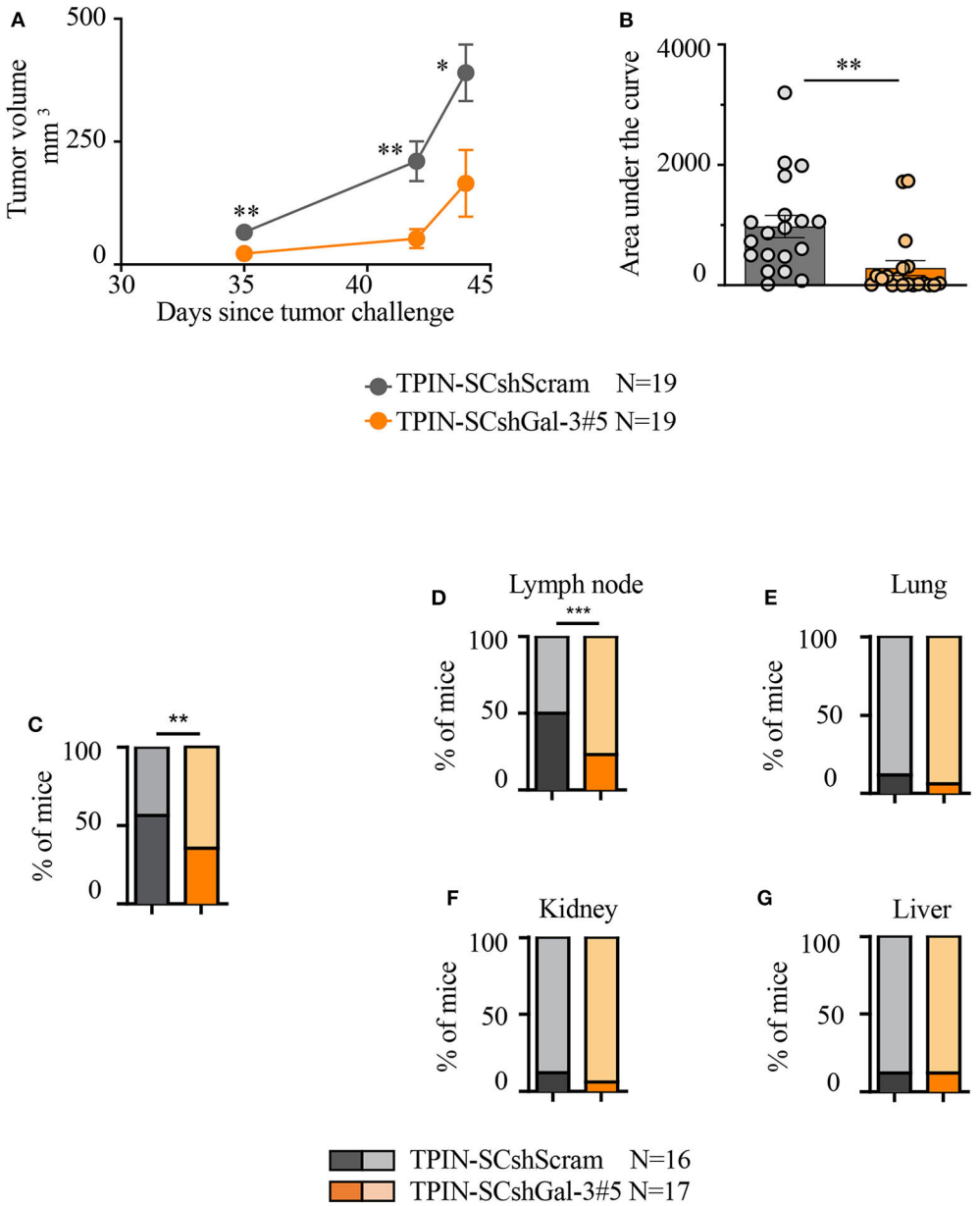

FIGURE 3 | Gal-3 impacts TPIN-SC tumorigenicity and metastatic potential. **(A)** Immunodeficient NSG mice received 2 × 10^6 TPIN-SCshScram or TPIN-SCshGal-3#5 (19 mice/group). The graph reports tumor growth (mm^3) progression volume. Average ± SEM of tumor volume. **(B)** The graph reports tumor progression expressed as area under the curve at day 44. Data are reported as a percentage ± SEM. Statistical analysis was performed using the Student *T*-test. Data represent a pool of four independent experiments. **(C)** When tumor area achieved ≥80 mm^2, the primary tumors were surgically resected to monitor metastatic spreading. The graph reports TPIN-SCshScram or TPIN-SCshGal-3#5 metastatic ability. **(D–G)** The graphs report the percentage of lymph node **(D)**, lung **(E)**, kidney **(F)**, liver **(G)**, metastatic spreading. Dark colors indicate metastasis-bearing mice, whereas light colors indicate metastasis-free mice. TPIN-SCshScram: $n = 16$ mice; TPIN-SCshGal-3#5: $n = 17$ mice. Statistical analysis was performed using the Fisher Exact Test. *$p < 0.05$; **$p < 0.01$; ***$p < 0.001$.

of the Oct4 promoter (48). Thus, only $Oct4^+$ cells expressed GFP. GFP^+ cells were sorted by flow cytometry to obtain a pure population of GFP^+ TPIN-SCs. Upon *in vitro* culture, GFP^+ TPIN-SCs progressively gave rise to ∼20% GFP^- TPIN-SCs, thus suggesting that the CSC core of GFP^+ TPIN-SCs autonomously and progressively re-establishes the heterogeneity found in prostaspheres, allowing some CSCs to differentiate by decreasing Oct4 expression (**Supplementary Figures 2A,B**). We focused on $Oct4^+$ TPIN-SCs, as they likely constitute highly undifferentiated CSCs. By ImageStream technology, we found that $Oct4^+$ TPIN-SCs had a pattern of intracellular Gal-3 distribution comparable to TPIN-SCs (**Figures 4C,D**). We conclude that TPIN-SCs are composed of CSCs that *in vitro* spontaneously generate a population of committed more differentiated precursors. Gal-3

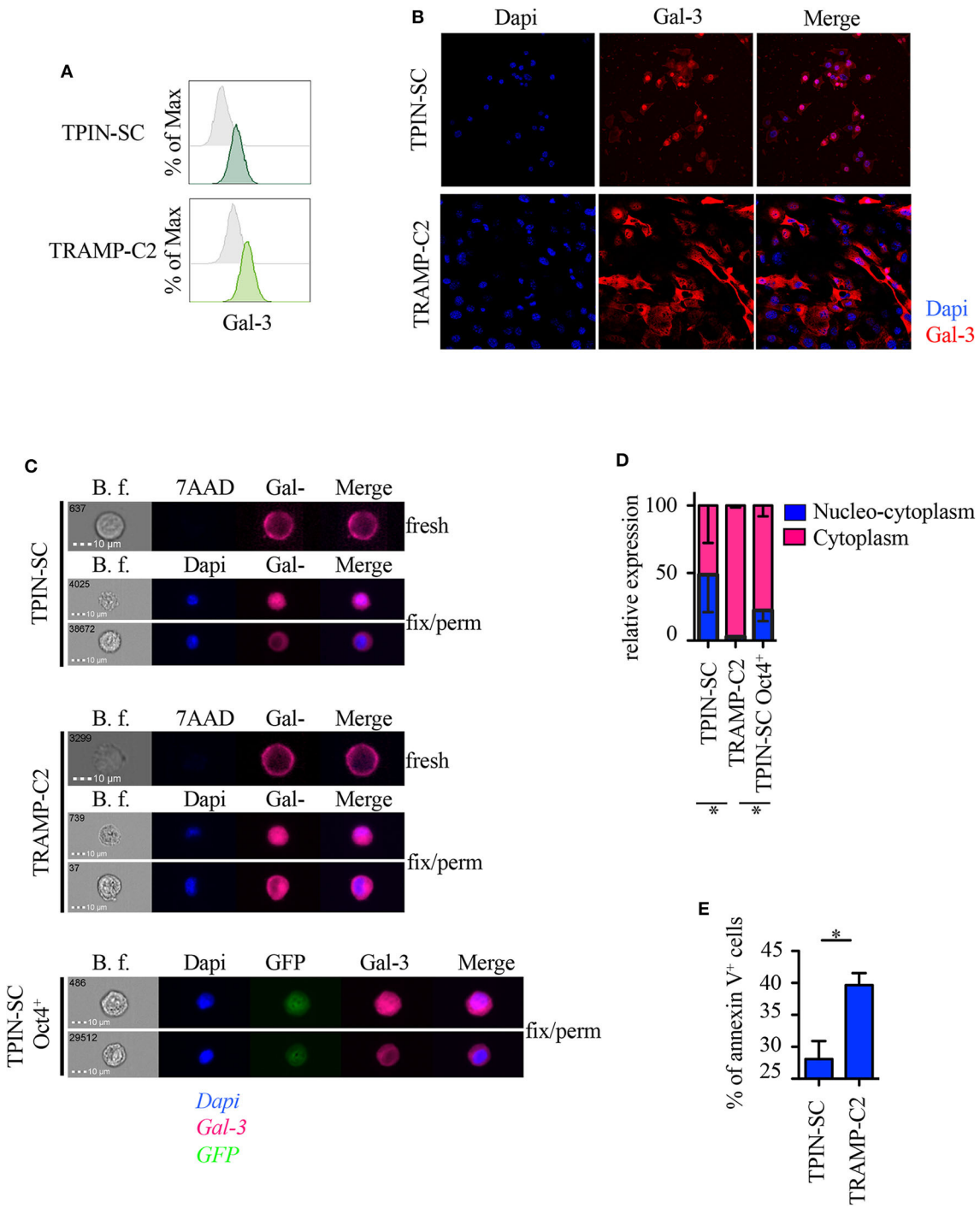

FIGURE 4 | Gal-3 is differently distributed in prostate CSCs and in more differentiated cancer cells. Expression of Gal-3 in the indicated mouse cells was assessed by flow cytometry analysis **(A)**, immunofluorescence **(B)** and ImageStream technology **(C)**. Fresh samples for cell surface detection of Gal-3 **(A,C)** were stained with 7AAD, while fixed and permeabilized samples for intracellular detection of Gal-3 were stained with Dapi **(B,C)**. In fresh samples for cell surface detection of Gal-3, dead cells were excluded by 7AAD positivity. Since we analyzed live cells only (thus, 7AAD negative), **(C)** does not show any 7AAD positivity. Cells were also stained with anti-Gal-3 antibodies. **(A)** Representative histograms of Gal-3 staining (green lines). Gray histograms: unstained. **(B)** Representative confocal images of Gal-3 staining. Red: Gal-3; Blue: Dapi. Magnification 63×. Images were optimized for brightness/contrast using imageJ. **(C)** Representative ImageStream images of Gal-3 staining. Magenta, Gal-3; Blue, Dapi; Green, GFP. **(D)** Quantification of Gal-3 intracellular distribution by ImageStream technology. Data are reported as relative expression of Gal-3 among the indicated cell lines; the blue bar reports the percentage of nucleo-cytoplasmic distribution of Gal-3, the magenta bar reports the percentage of mainly cytoplasmic distribution of Gal-3. Statistical analysis was performed using Student *T*-test. The panel is a pool of three independent experiments. **(E)** Quantification of Annexin V^+ cells analyzed by flow cytometry in the reported cell lines. Statistical analysis was performed using Student *T*-test. The panel reports one experiment representative of three independent experiments. *$p < 0.05$.

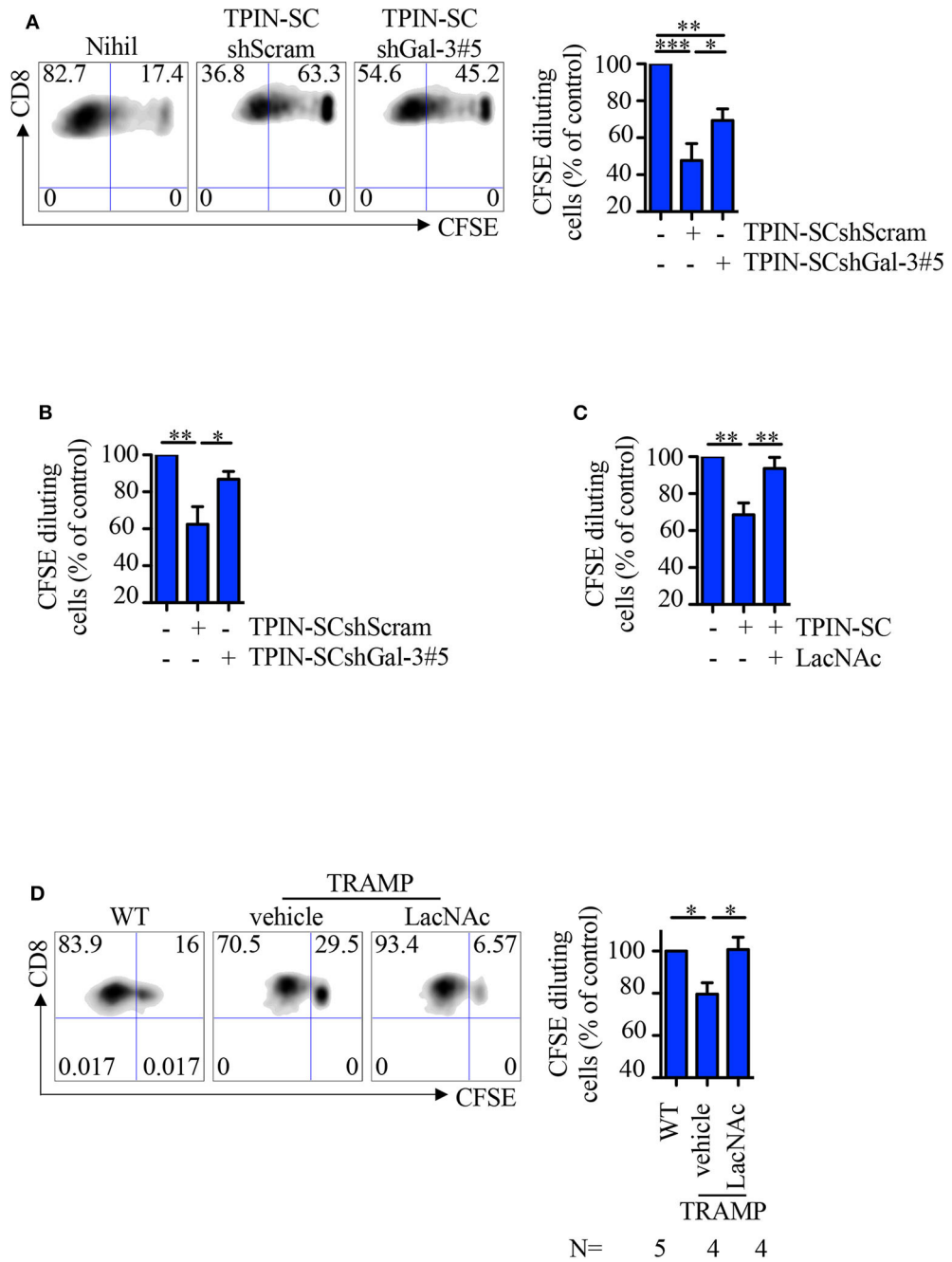

FIGURE 5 | TPIN-SC use Gal-3 to dampen T cell proliferation. Naïve **(A,C)** or RAG-OT1 **(B)** splenocytes were labeled with CFSE, and activated with anti-CD3 and anti-CD28 beads **(A,C)** or OVA **(B)**, respectively, in the presence or absence of irradiated TPIN-SC cells **(C)**, or TPIN-SC infected with lentiviral vectors encoding Gal-3-specific shRNA [TPIN-SCshGal-3#5 **(A,B)**] or unspecific [TPIN-SCshScram **(A,B)**]. Where indicated, 5 mM LacNAc was added to the culture **(C)**. Representative dot plots of CFSE dilution for each experimental condition **(A)** and quantification of CFSE dilution reported as percentage of CD8 proliferating T cells at day 4 **(A,C)** or day 3 **(B)**. Values were normalized to the positive control (splenocytes activated with anti-CD3 and anti-CD28 beads or OVA). Statistical analysis was performed using Anova followed by Tukey's test or Student *T*-test. Graph **(A)** is a pool of nine independent experiments; graph **(B)** is a pool of four independent experiments; graph **(C)** is a pool of six independent experiments. **(D)** CFSE dilution of CD8 T cells from prostate-draining lymph nodes of 12/13-week-old TRAMP and wild type (WT) mice at day 3 of stimulation with anti-CD3/CD28 beads. Cells from TRAMP-derived prostate-draining lymph nodes were subdivided in two parts, one of which was also incubated with 5 mM LacNAc. Representative dot plots of CFSE dilution for each experimental condition, and quantification of the percentage of CD8 proliferating T cells at day 3. Each panel is representative of at least two independent experiments. Values were normalized to the positive control (WT). Statistical analysis was performed using Anova followed by Tukey's test. The graph is a pool of four independent experiments. $^{*}p < 0.05$; $^{**}p < 0.01$; $^{***}p<0.001$.

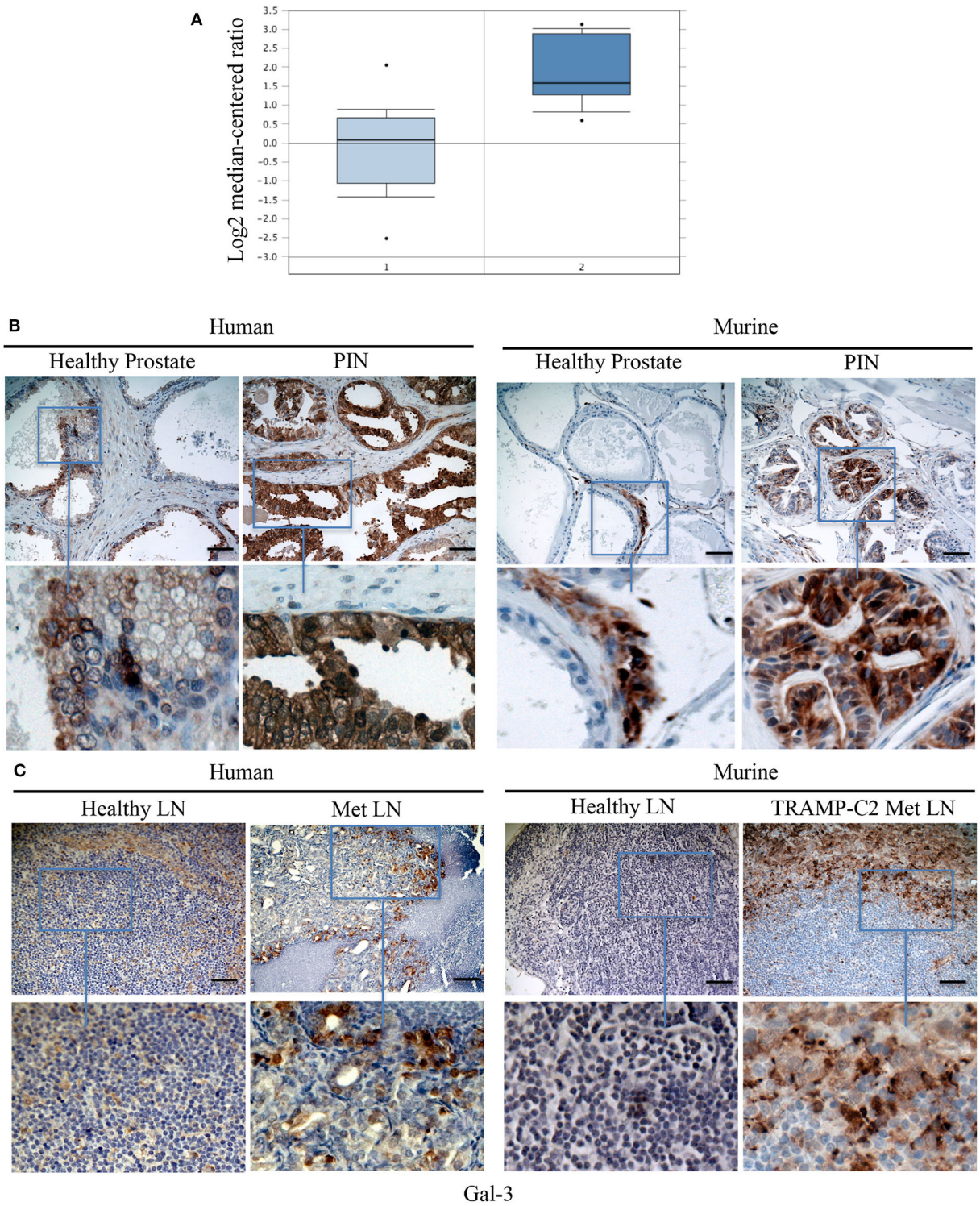

FIGURE 6 | Gal-3 is expressed in human and mouse PIN lesions and metastatic lymph nodes. **(A)** The levels of Gal-3 transcripts in normal and cancerous human prostate carcinoma tissues. Raw data were retrieved from the Oncomine (www.oncomine.org), Tomlins Prostate Dataset (50). Transcript level of Gal-3 in PIN samples (2), $n = 13$, was compared with samples prostate gland (1), $n = 23$. Box plot represents the median with 90th and 10th percentiles, and statistical significance was analyzed by Student T-test, $p = 0.00307$. Formalin fixed paraffin embedded sections from human and mouse: healthy prostate and PIN lesions **(B)** or healthy and metastatic (Met) lymph nodes (LN) **(C)** were stained by immunohistochemistry in order to evaluate Gal 3 expression. Scale Bar = 20 mm. In blue boxes zoom details. Slides are representative of at least three different cases. Images were optimized for brightness.

has a preferential cytoplasmic and nuclear localization in TPIN-SCs, irrespective of their differentiation stage.

Because Gal-3 may favor or protect from apoptosis depending on its intracellular localization (10), we investigated apoptosis in TPIN-SCs and the more differentiated TRAMP-C2 cells. TPIN-SCs were less prone to undergo apoptosis than TRAMP-C2 cells (**Figure 4E**, **Supplementary Figure 3**), thus suggesting that nucleus-cytoplasmic distribution of Gal-3 in CSCs protect them from apoptosis.

TPIN-SCs Use Gal-3 to Dampen T Cell Proliferation

Because Gal-3 is immunosuppressive (11), we asked if TPIN-SCs utilize Gal-3, together with Tenascin-C (30), to suppress T cell-mediated immune responses. To this aim, CD8 T cells from the spleen of naive or TCR transgenic RAG-OT1 mice were labeled with CFSE, and stimulated with anti-CD3/CD28 beads or the $OVA_{257-264}$ peptide, respectively, in the presence of prostate CSCs. Whereas, as expected (30), the addition of TPIN-SCshScram to the culture blocked T cell proliferation, Gal-3 silencing in TPIN-SCs substantially dampened their immunomodulatory effects (**Figures 5A,B**). The direct immunomodulatory role of Gal-3 was confirmed by adding the Gal-3 synthetic inhibitor LacNAc (49) to the co-culture with TPIN-SCs, and showing that CD8 T cell proliferation was rescued (**Figure 5C**).

We previously showed that CSCs precociously migrate to prostate-draining lymph nodes of TRAMP mice affected by PIN through the CXCR4/CXCL12 axis, and participate in generating a local immunosuppressive microenvironment (30, 46). Indeed, CD8 T cells obtained from prostate-draining lymph nodes of TRAMP mice proliferated less than T cells from prostate-draining lymph nodes of age-matched wild type littermates (**Figure 5D**). To investigate if Gal-3 was responsible for this phenomenon, CFSE-labeled naïve cells from prostate-draining lymph nodes of TRAMP mice were cultured with anti-CD3/CD28 beads and LacNAc (**Figure 5D**). Flow cytometry analysis of CD8 T cells showed that in the presence of LacNAc, T cell proliferation was restored to the levels of T cell proliferation in age-matched wild type mice, thus confirming that Gal-3 contributes to the immunosuppressive milieu in TRAMP lymph nodes. Altogether, these findings suggest that Gal-3 participates to the immunosuppressive activity of TPIN-SCs both in the primary tumor lesion and in precociously invaded lymph nodes.

Gal-3 Is Expressed in Human and Mouse PIN Lesions and Metastatic Lymph Nodes

Because TPIN-SCs originate from PIN lesions, we searched for a published gene signature of human normal prostate and PIN (50). As reported in **Figure 6A**, the Gal-3 transcript was found overexpressed in human PIN when compared to healthy prostate. We next validated Gal-3 expression at the protein level by immunohistochemistry. While in the healthy human and mouse prostate, Gal-3 showed a weak immunostaining primarily localized in the cytoplasm (**Figure 6B**), in human PIN lesions Gal-3 staining was rather heterogeneous and intense, and mainly cytoplasmic (**Figure 6B**), thus confirming previous findings (14). Interestingly, Gal-3 was also found in mouse PIN lesions, where it showed a patchy distribution (**Figure 6B**). Thus, both human and murine PIN lesions express Gal-3 preferentially in the cytoplasm of transformed cells, as we found in differentiated TRAMP-C2 cells (**Figure 4**).

Based on our findings in the TRAMP model (**Figure 3**), and the known role of Gal-3 in the metastatic process (51), we were interested in investigating the expression of Gal-3 in metastatic prostate cancer. To this aim, we stained with anti-Gal-3 antibodies human Du145 cells, which were derived from a central nervous system metastasis (35), and PC3 cells obtained from a metastatic lymph node (36). At flow cytometry, both cell populations clearly expressed Gal-3 (**Supplementary Figure 4**). By immunohistochemistry we found that Gal-3 was strongly expressed in metastatic bone from prostate cancer patients (**Figure 6C** and **Table 1**), thus confirming previous findings (52). We also originally observed that in some samples Gal-3 staining was stronger at the invading edge of lymph node metastasis (**Figure 6C** and **Table 1**).

We also investigated Gal-3 expression in mouse lymph nodes affected by measurable metastasis. The incidence of measurable lymph node metastasis in TRAMP mice has been reported to be very low (30, 53). A recent survey in our colony of 88 TRAMP mice found lymph node metastases by adenocarcinoma, which were confirmed by the pathologist, in two mice, accounting for ∼3% of the screened animals. To overcome the limitation of the autochthonous TRAMP model, we took advantage of the well-established model of lymph node metastasis upon subcutaneous challenge with TRAMP-C2 cells (39). Thus, C57BL/6 mice were challenged with TRAMP-C2 cells (**Supplementary Figure 5**). When the tumor area reached $\geq$80 mm^2, we surgically resected the primary tumor, and monitored mice for lymph node metastasis occurrence. Approximately 1 month after surgery, 86% of the mice (i.e., six out of seven mice) developed axillary and inguinal lymph node metastases. In 62% of the metastatic lymph nodes from TRAMP-C2-challenged mice we found Gal-3 expression in neoplastic cells invading the lymph node (**Table 1**). Similarly to the human counterpart, 25% of metastatic lymph nodes from TRAMP-C2-challenged mice had a more intense Gal-3 staining at the invading edge of the metastasis (**Figure 6C** and **Table 1**). Altogether, these findings demonstrate that Gal-3 is expressed in human and murine PIN lesions as well as in metastatic lymph nodes.

TABLE 1 | Gal-3 expression in tumor cells invading metastatic lymph nodes.

	Gal-3$^+$samples (%)	Gal-3 at leading edge (%)
Human	9/9 (100)	2/9 (22)
Mouse	8/13 (62)	2/8 (25)

Number of human and mouse metastatic lymph nodes stained for Gal-3 by immunohistochemistry. Human samples: pelvic lymph nodes from 9 patients. Murine samples: axillary/inguinal lymph nodes from 7 mice challenged with TRAMP-C2 cells. Leading edge refers to intense Gal-3 staining in cancer cells at the interface with lymphocytes in lymph nodes.

DISCUSSION

Prostate cancer is one of the most frequently diagnosed cancers, and it accounts for 19% of all estimated new cancer cases in men (54). Metastatic dissemination is a severe complication of prostate cancer, and the main cause of cancer mortality. The majority of prostate cancer patients harbor bone with lymph-node metastases, 6% develop exclusive lymph node disease recurrence and 20% have visceral metastases (55). When prostate cancer becomes castration-resistant it is essentially incurable. Indeed, prostate cancer is one of the major causes of death by cancer and accounts for 9% of estimated cancer deaths in men (54). Thus, a better understanding of the metastatic process in prostate cancer is essential to direct current and future therapeutic strategies.

The prostate cancer microenvironment is immunosuppressive (56, 57). We and others have previously reported that in TRAMP mice, especially in the early phases of cancer development and progression (33, 58), the tumor microenvironment is endowed with redundant immunosuppressive mechanisms. These are operated by several cell populations, including regulatory T cells (59, 60), myeloid derived suppressor cells (61, 62), and prostate CSCs (30). Our new findings suggest that Gal-3 is an additional mechanism of immune suppression that acts both in primary prostate lesions and in lymph nodes. Gal-3 also exerts pro-metastatic functions in CSCs. Several experimental evidences support our conclusions. Firstly, Gal-3 expressed in TPIN-SCs dampened T cell proliferation, and Gal-3 silencing in TPIN-SCs or the addition of LacNac to the co-culture recued T cell proliferation. Gal-3 silencing in TPIN-SCs also diminished *in vitro* cell proliferation, thus substantiating a direct function of Gal-3 in supporting proliferation not only of differentiated cancer cells (18), but also of prostate CSCs, as previously described for other CSCs (23, 26). More importantly, Gal-3 impacted TPIN-SC proliferative potential also *in vivo*, as Gal-3 silencing in TPIN-SC reduced tumor burden. Thus, our findings confirm data obtained *in vitro* and *in vivo* with PC3 cells (18), and extend the role of Gal-3 to prostate CSCs. Gal-3 also supported the metastatic potential of TPIN-SCs, and when expressed in TPIN-SCs, Gal-3 endowed prostate CSCs with tropism for draining lymph nodes. Hence, when expressed in prostate CSCs, Gal-3 supports tumor growth and metastatic dissemination through cell-intrinsic and cell-extrinsic mechanisms (**Figure 7**). It will be interesting to identify the molecular mechanism by which Gal-3 endows CSCs with metastatic potential.

Gal-3 has been already implicated in the biology of prostate cancer (12), and Gal-3 has been proposed as predictive biomarker of prostate cancer aggressiveness especially in the context of metastasis (20, 21). Our analyses on human and mouse tissues confirm and extend previous findings showing that Gal-3 is expressed in both human and mouse PIN lesions, as well as in metastases (13–17, 63). All together, these findings suggest that Gal-3 has a relevant role already at the stage of PIN. Whereas, in humans a direct link between PIN and prostate adenocarcinoma has not been demonstrated, in TRAMP mice, PIN invariably precedes adenocarcinoma (31). Because Gal-3 is expressed in mouse PIN lesions, prostate CSCs and lymph node metastasis, we hypothesize that Gal-3 links mouse PIN lesions to lymph node metastasis *via* CSCs. By acting directly on CSCs and indirectly on immune surveillance, Gal-3 might favor the precocious dissemination of the former.

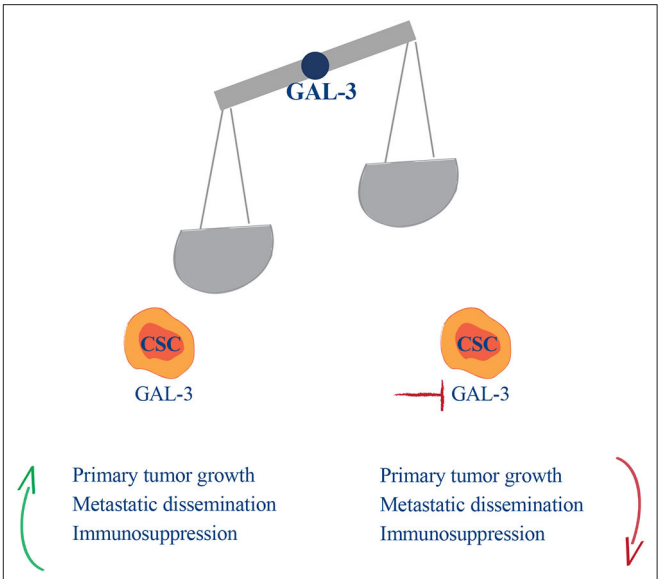

FIGURE 7 | Gal-3 balances cancer malignancy in the early phases of prostate cancer development. In the early phases of disease development and metastasis CSCs, through Gal-3, drive prostate cancer malignancy, and immunosuppression.

The finding that adenocarcinoma metastases are rare, but prostate CSCs can frequently be isolated from prostate draining lymph nodes of TRAMP mice is only apparently contradicting. In fact, autochthonous tumors in TRAMP mice lack genetic alterations that drive full prostate cancer metastatization (64). Nonetheless, our findings in the TRAMP model support a process of early lymph node seeding by prostate CSCs, and let us hypothesize that in some prostate cancer patients, metastasis occurs very early, and may account for recurrence after radical prostatectomy (65). Thus, measuring Gal-3 expression in prostate biopsies and/or Gal-3 levels in blood might be an early predictor of metastatic disease. This hypothesis requires investigation in a prospective clinical trial.

Importantly, a more intense Gal-3 staining was found at the leading edge of lymph node metastasis in some human and mouse samples. These findings further support a relevant role for Gal-3 in the invading process, and let us hypothesize that the leading edge is rich in CSCs. Because flow cytometry and immunohistochemistry analyses showed that Gal-3 expression is not restricted to CSCs, an alternative hypothesis is that Gal-3 might be upregulated in more invading tumor cells irrespective of their differentiation status. We are currently investigating between these two non-mutually exclusive possibilities.

Gal-3 overexpression at the leading edge of the lymph node metastasis, where cancer cells and lymphocytes get directly in contact, might also exert an important immunomodulatory activity. In support of this hypothesis, we have found that either silencing Gal-3 in TPIN-SC or the addition of LacNAc to the

cultures rescued T cell proliferation in the presence of TPIN-SCs. More importantly, incubation of T cells with LacNAc rescued T cell proliferation in prostate-draining lymph nodes of TRAMP mice affected by mouse PIN. Thus, CSCs that early migrated to prostate-draining lymph nodes contributed to the establishment of an immunosuppressive milieu (30, 46) also through Gal-3. LacNAc in prostate-draining lymph nodes might inhibit Gal-3 either drained through lymphatic vessels from the primary tumor lesion, or locally produced by migrated prostate CSCs. Against the former hypothesis are evidences that inhibition of CSCs migration to prostate-draining lymph nodes avoids local immune suppression (30), and that CSCs require a cell-to-cell contact to dampen T cell activation (30).

Silencing of either Tenascin-C or Gal-3 in TPIN-SCs only partially rescued T cell proliferation, suggesting that the two molecules are endowed with different and potentially independent immunosuppressive mechanisms. In fact, Tenascin-C binds to α5β1 integrin expressed on the cell surface of both human and mouse T cells (30, 46), and inhibits stress fiber formation, thus dampening T cell receptor-dependent activation, proliferation, and cytokine production. Gal-3 has been reported to impair T cell activation by destabilizing the immunological synapse (66), and inhibiting TCR clustering (67) and CD8-TCR interactions (49). Our findings, however, do not exclude interactions between Gal-3 and Tenascin-C in favoring prostate CSCs tumorigenic and metastatic potential. As an example, by interacting with N-linked oligosaccharides on the surface of mammary carcinoma cells, Gal-3 induces activation of α5β1 integrin, the target of Tenascin-C on T cells (30), favoring, in this case, fibronectin fibrillogenesis, and fibronectin-dependent spreading and motility of tumor cells (68). Additionally, Gal-3 is able to directly interact with Tenascin-C (69), and the two molecules have been involved in homotypic cancer cell adhesion in glioma (70). Analogously, we speculate that Gal-3 and Tenascin-C may directly interact, thus mediating important steps of the metastatic cascade in prostate cancer.

The consistent number of Gal-3$^+$ cells both in PIN lesions and in metastatic lymph nodes suggests that Gal-3 expression is not restricted to CSCs, and indeed, we have found that Gal-3 is also produced by more differentiated human and murine prostate cancer cells. Interestingly, intracellular distribution of Gal-3 appears to vary depending on the differentiation state of the cancer cells. While in less differentiated prostate CSCs, Gal-3 was equally distributed in nucleus and cytoplasm, in more differentiated cells Gal-3 was preferentially confined to the cytoplasm. In support of the latter finding, in most of the tumor cells in PIN and metastatic lesions, Gal-3 is cytoplasmic. The role of nuclear and cytoplasmic Gal-3 expression in prostate CSCs still need to be investigated. Within the cell, Gal-3 can shuttle between the nucleus and the cytoplasm, thus participating to cell cycle progression, cell growth, and apoptosis (18). We analyzed the apoptotic process in culture conditions, and found that TRAMP-C2 cells were more prone to apoptosis than CSCs, thus suggesting that nucleus-cytoplasm distribution of Gal-3 protects CSCs from apoptosis. This finding was unexpected, as cytoplasmic Gal-3 has been previously described to protect from apoptosis (71). Galectins can undergo post-translational proteolysis and phosphorylation (72), which might depend on the redox status of the microenvironment (73). Upon phosphorylation, Gal-3 acquires its anti-apoptotic and cell cycle arrest functions (74). Thus, we speculate that the culture conditions in which TRAMP-C2 cells were grown did not allow adequate post-translational modification of Gal-3. We also hypothesize that nuclear Gal-3 exclusion may associate with cell cycle progression in more differentiated prostate cancer cells. Thus, equal distribution of Gal-3 in the two cell compartments may favor CSC quiescence, and identify CSCs in prostate cancer. Further investigation is required to support our hypotheses.

Bresalier et al. (22) used surface Gal-3 expression as marker of CSCs in gastrointestinal tumors. Because we have found that both CSCs and more differentiated human and mouse prostate cancer cells express Gal-3 on the cell surface, surface Gal-3 does not appear to represent a stemness marker in prostate cancer.

Several Gal-3-specific therapeutic strategies are available (75). *In vitro*, PectaSol-C Modified Citrus Pectin and GCS-100 induced apoptosis, inhibition of cell proliferation and cell cycle arrest in cancer cells from the prostate and other tumors (76–78). Additionally, treatment with GCS-100 overcame the Gal-3-induced disfunction of tumor infiltrating T cells, and favored tumor rejection in mice (79). It has also been reported that the Thomsen-Friedenreich disaccharide TFD100 purified from cod blocked Gal-3-mediated angiogenesis and prostate cancer metastasis in mice, as well as apoptosis of activated T cells (80). Treatment with the Gal-3 inhibitor GR-MD-02 in combination with the stimulatory anti-OX40 monoclonal antibody promoted antigen specific T cell expansion and survival of mice bearing TRAMP-C1 tumors, reduced lung metastases in the 4T1 model, and showed anti-tumor activity in other mouse models (81). Gal-3 inhibitors, used either alone or in combination with immune checkpoint blockers or vaccination, have been and also are investigated in phase I-III clinical trials in melanoma, non-small cell lung cancer, squamous cell carcinoma of the head and neck, and chronic lymphocytic leukemia (NCT02575404, NCT02117362, NCT01723813, and NCT00514696). PectaSol-C Modified Citrus Pectin is proposed as dietary supplement in biochemical relapsed prostate cancer-affected patients [NCT01681823; refs. (75, 82)]. Our findings support the hypothesis that Gal-3 inhibitors also target CSCs, and could be tested in the early phases of prostate cancer.

DATA AVAILABILITY STATEMENT

The dataset has been uploaded to the GEO - GSE65502. Other raw data supporting the conclusions of this article will be made available by the authors, without undue reservation, to any qualified researcher.

ETHICS STATEMENT

The studies involving human participants were reviewed and approved by Comitato Etico Ospedale San Raffaele. The patients/participants provided their written informed consent to participate in this study. The animal study was reviewed and approved by Institutional Ethical Committee, San Raffaele Hospital.

AUTHOR CONTRIBUTIONS

MB developed the concept of the study. MB, EJ, SC, ABre, AE, and CB designed and conceived the experiments. SC, MG, ABre, TB, AM, VP, AE, CB, and EJ performed the experiments. MG took care of the mouse colonies. AL supervised the experiments conducted to generate TPIN-SCkoGal-3 and TPIN-SCkoScram cell lines. IP analyzed microarray data. RG supervised western blot analyses. ABri provided patients samples. MF and CD supervised preparation of immunohistochemistry samples and analyzed them. SC and ABre prepared the figures and tables. MB and SC wrote and prepared the manuscript. All authors read and approved the manuscript.

FUNDING

This work was supported by Associazione Italiana per la Ricerca sul Cancro (AIRC; Grant No. #IG16807 to MB). SC and ABre were supported by fellowships from the Fondazione Italiana per la Ricerca sul Cancro/AIRC (Grants #18314 to SC and #22316 to ABre).

ACKNOWLEDGMENTS

The authors acknowledge the Advanced Light and Electron Microscopy Bioimaging Center (ALEMBIC) (San Raffaele Scientific Institute, Milan, Italy) for excellent support in image acquisition; Dr. Vincenzo Russo and Dr. Raffaella C. Fontana (San Raffaele Scientific Institute, Milan, Italy) and Dr. Dario Sangiolo (Università degli Studi di Torino, Turin, Italy) for the help on lentiviral transduction with the vector carrying the GFP sequence under the control of the Oct4 promoter (San Raffaele Scientific Institute, Milan, Italy); Dr. Ilaria Malanchi (The Francis Crick Institute, London, England), and Dr. Giorgio Stassi (University Of Palermo, Palermo, Italy) for critical comments and helpful suggestions. SC conducted this study in partial fulfillment of her Ph.D. at San Raffaele University.

SUPPLEMENTARY MATERIAL

The Supplementary Material for this article can be found online at: https://www.frontiersin.org/articles/10.3389/fimmu.2020.01820/full#supplementary-material

REFERENCES

1. Maman S, Witz IP. A history of exploring cancer in context. *Nat Rev Cancer*. (2018) 18:359–76. doi: 10.1038/s41568-018-0006-7
2. Visvader JE, Lindeman GJ. Cancer stem cells: current status and evolving complexities. *Cell Stem Cell*. (2012) 10:717–28. doi: 10.1016/j.stem.2012.05.007
3. Chaffer CL, Weinberg RA. How does multistep tumorigenesis really proceed? *Cancer Discov*. (2015) 5:22–4. doi: 10.1158/2159-8290.CD-14-0788
4. Turley SJ, Cremasco V, Astarita JL. Immunological hallmarks of stromal cells in the tumour microenvironment. *Nat Rev Immunol*. (2015) 15:669–82. doi: 10.1038/nri3902
5. Hinshaw DC, Shevde LA. The tumor microenvironment innately modulates cancer progression. *Cancer Res*. (2019) 79:4557–66. doi: 10.1158/0008-5472.CAN-18-3962
6. De Palma M, Biziato D, Petrova TV. Microenvironmental regulation of tumour angiogenesis. *Nat Rev Cancer*. (2017) 17:457–74. doi: 10.1038/nrc.2017.51
7. Hamidi H, Ivaska J. Every step of the way: integrins in cancer progression and metastasis. *Nat Rev Cancer*. (2018) 18:533–48. doi: 10.1038/s41568-018-0038-z
8. Yang RY, Rabinovich GA, Liu FT. Galectins: structure, function and therapeutic potential. *Expert Rev Mol Med*. (2008) 10:e17. doi: 10.1017/S1462399408000719
9. Ruvolo PP. Galectin 3 as a guardian of the tumor microenvironment. *Biochim Biophys Acta*. (2016) 1863:427–37. doi: 10.1016/j.bbamcr.2015.08.008
10. Liu FT, Rabinovich GA. Galectins as modulators of tumour progression. *Nat Rev Cancer*. (2005) 5:29–41. doi: 10.1038/nrc1527
11. Hsu DK, Chen HY, Liu FT. Galectin-3 regulates T-cell functions. *Immunol Rev*. (2009) 230:114–27. doi: 10.1111/j.1600-065X.2009.00798.x
12. Martinez-Bosch N, Rodriguez-Vida A, Juanpere N, Lloreta J, Rovira A, Albanell J, et al. Galectins in prostate and bladder cancer: tumorigenic roles and clinical opportunities. *Nat Rev Urol*. (2019) 16:433–45. doi: 10.1038/s41585-019-0183-5
13. Pacis RA, Pilat MJ, Pienta KJ, Wojno K, Raz A, Hogan V, et al. Decreased galectin-3 expression in prostate cancer. *Prostate*. (2000) 44:118–23. doi: 10.1002/1097-0045(20000701)44:2<118::AID-PROS4>3.0.CO;2-U
14. Van Den Brule FA, Waltregny D, Liu FT, Castronovo V. Alteration of the cytoplasmic/nuclear expression pattern of galectin-3 correlates with prostate carcinoma progression. *Int J Cancer*. (2000) 89:361–7. doi: 10.1002/1097-0215(20000720)89:4<361::AID-IJC8>3.0.CO;2-U
15. Merseburger AS, Kramer MW, Hennenlotter J, Simon P, Knapp J, Hartmann JT, et al. Involvement of decreased galectin-3 expression in the pathogenesis and progression of prostate cancer. *Prostate*. (2008) 68:72–7. doi: 10.1002/pros.20688
16. Knapp JS, Lokeshwar SD, Vogel U, Hennenlotter J, Schwentner C, Kramer MW, et al. Galectin-3 expression in prostate cancer and benign prostate tissues: correlation with biochemical recurrence. *World J Urol*. (2013) 31:351–8. doi: 10.1007/s00345-012-0925-y
17. Ahmed H, Cappello F, Rodolico V, Vasta GR. Evidence of heavy methylation in the galectin 3 promoter in early stages of prostate adenocarcinoma: development and validation of a methylated marker for early diagnosis of prostate cancer. *Transl Oncol*. (2009) 2:146–56. doi: 10.1593/tlo.09118
18. Wang Y, Nangia-Makker P, Tait L, Balan V, Hogan V, Pienta KJ, et al. Regulation of prostate cancer progression by galectin-3. *Am J Pathol*. (2009) 174:1515–23. doi: 10.2353/ajpath.2009.080816
19. Pienta KJ, Naik H, Akhtar A, Yamazaki K, Replogle TS, Lehr J, et al. Inhibition of spontaneous metastasis in a rat prostate cancer model by oral administration of modified citrus pectin. *J Natl Cancer Inst*. (1995) 87:348–53. doi: 10.1093/jnci/87.5.348
20. Balan V, Wang Y, Nangia-Makker P, Kho D, Bajaj M, Smith D, et al. Galectin-3: a possible complementary marker to the PSA blood test. *Oncotarget*. (2013) 4:542–9. doi: 10.18632/oncotarget.923
21. Nakajima K, Heilbrun LK, Hogan V, Smith D, Heath E, Raz A. Positive associations between galectin-3 and PSA levels in prostate cancer patients: a prospective clinical study-I. *Oncotarget*. (2016) 7:82266–72. doi: 10.18632/oncotarget.12619
22. Ilmer M, Mazurek N, Byrd JC, Ramirez K, Hafley M, Alt E, et al. Cell surface galectin-3 defines a subset of chemoresistant gastrointestinal tumor-initiating cancer cells with heightened stem cell characteristics. *Cell Death Dis*. (2016) 7:e2337. doi: 10.1038/cddis.2016.239
23. Kang HG, Kim DH, Kim SJ, Cho Y, Jung J, Jang W, et al. Galectin-3 supports stemness in ovarian cancer stem cells by activation of the Notch1 intracellular domain. *Oncotarget*. (2016) 7:68229–41. doi: 10.18632/oncotarget.11920
24. Kuo HY, Hsu HT, Chen YC, Chang YW, Liu FT, Wu CW. Galectin-3 modulates the EGFR signalling-mediated regulation of Sox2 expression via c-Myc in lung cancer. *Glycobiology*. (2016) 26:155–65. doi: 10.1093/glycob/cwv088

25. Huang CS, Tang SJ, Lee MH, Chang Wang CC, Sun GH, Sun KH. Galectin-3 promotes CXCR2 to augment the stem-like property of renal cell carcinoma. *J Cell Mol Med*. (2018) 22:5909–18. doi: 10.1111/jcmm.13860
26. Nangia-Makker P, Hogan V, Raz A. Galectin-3 and cancer stemness. *Glycobiology*. (2018) 28:172–81. doi: 10.1093/glycob/cwy001
27. Oskarsson T, Batlle E, Massague J. Metastatic stem cells: sources, niches, and vital pathways. *Cell Stem Cell*. (2014) 14:306–21. doi: 10.1016/j.stem.2014.02.002
28. Klein CA. Parallel progression of primary tumours and metastases. *Nat Rev Cancer*. (2009) 9:302–12. doi: 10.1038/nrc2627
29. Mazzoleni S, Jachetti E, Morosini S, Grioni M, Piras IS, Pala M, et al. Gene signatures distinguish stage-specific prostate cancer stem cells isolated from transgenic adenocarcinoma of the mouse prostate lesions and predict the malignancy of human tumors. *Stem Cells Transl Med*. (2013) 2:678–89. doi: 10.5966/sctm.2013-0041
30. Jachetti E, Caputo S, Mazzoleni S, Brambillasca CS, Parigi SM, Grioni M, et al. Tenascin-C protects cancer stem-like cells from immune surveillance by arresting T-cell activation. *Cancer Res*. (2015) 75:2095–108. doi: 10.1158/0008-5472.CAN-14-2346
31. Greenberg NM, Demayo F, Finegold MJ, Medina D, Tilley WD, Aspinall JO, et al. Prostate cancer in a transgenic mouse. *Proc Natl Acad Sci USA*. (1995) 92:3439–43. doi: 10.1073/pnas.92.8.3439
32. Mombaerts P, Iacomini J, Johnson RS, Herrup K, Tonegawa S, Papaioannou VE. RAG-1-deficient mice have no mature B and T lymphocytes. *Cell*. (1992) 68:869–77. doi: 10.1016/0092-8674(92)90030-G
33. Degl'innocenti E, Grioni M, Boni A, Camporeale A, Bertilaccio MT, Freschi M, et al. Peripheral T cell tolerance occurs early during spontaneous prostate cancer development and can be rescued by dendritic cell immunization. *Eur J Immunol*. (2005) 35:66–75. doi: 10.1002/eji.200425531
34. Foster BA, Gingrich JR, Kwon ED, Madias C, Greenberg NM. Characterization of prostatic epithelial cell lines derived from transgenic adenocarcinoma of the mouse prostate (TRAMP) model. *Cancer Res*. (1997) 57:3325–30.
35. Stone KR, Mickey DD, Wunderli H, Mickey GH, Paulson DF. Isolation of a human prostate carcinoma cell line (DU 145). *Int J Cancer*. (1978) 21:274–81. doi: 10.1002/ijc.2910210305
36. Kaighn ME, Narayan KS, Ohnuki Y, Lechner JF, Jones LW. Establishment and characterization of a human prostatic carcinoma cell line (PC-3). *Invest Urol*. (1979) 17:16–23.
37. Hess Michelini R, Freschi M, Manzo T, Jachetti E, Degl'innocenti E, Grioni M, et al. Concomitant tumor and minor histocompatibility antigen-specific immunity initiate rejection and maintain remission from established spontaneous solid tumors. *Cancer Res*. (2010) 70:3505–14. doi: 10.1158/0008-5472.CAN-09-4253
38. Iezzi G, Boni A, Degl'innocenti E, Grioni M, Bertilaccio MT, Bellone M. Type 2 cytotoxic T lymphocytes modulate the activity of dendritic cells toward type 2 immune responses. *J Immunol*. (2006) 177:2131–7. doi: 10.4049/jimmunol.177.4.2131
39. Kwon ED, Foster BA, Hurwitz AA, Madias C, Allison JP, Greenberg NM, et al. Elimination of residual metastatic prostate cancer after surgery and adjunctive cytotoxic T lymphocyte-associated antigen 4 (CTLA-4) blockade immunotherapy. *Proc Natl Acad Sci USA*. (1999) 96:15074–9. doi: 10.1073/pnas.96.26.15074
40. Elia AR, Grioni M, Basso V, Curnis F, Freschi M, Corti A, et al. Targeting tumor vasculature with TNF leads effector T cells to the tumor and enhances therapeutic efficacy of immune checkpoint blockers in combination with adoptive cell therapy. *Clin Cancer Res*. (2018) 24:2171–81. doi: 10.1158/1078-0432.CCR-17-2210
41. Lombardo A, Cesana D, Genovese P, Di Stefano B, Provasi E, Colombo DF, et al. Site-specific integration and tailoring of cassette design for sustainable gene transfer. *Nat Methods*. (2011) 8:861–9. doi: 10.1038/nmeth.1674
42. Cantore A, Ranzani M, Bartholomae CC, Volpin M, Valle PD, Sanvito F, et al. Liver-directed lentiviral gene therapy in a dog model of hemophilia B. *Sci Transl Med*. (2015) 7:277ra228. doi: 10.1126/scitranslmed.aaa1405
43. Sorrentino C, Ciummo SL, Cipollone G, Caputo S, Bellone M, Di Carlo E. Interleukin-30/IL27p28 shapes prostate cancer stem-like cell behavior and is critical for tumor onset and metastasization. *Cancer Res*. (2018) 78:2654–68. doi: 10.1158/0008-5472.CAN-17-3117
44. Jachetti E, Mazzoleni S, Grioni M, Ricupito A, Brambillasca C, Generoso L, et al. Prostate cancer stem cells are targets of both innate and adaptive immunity and elicit tumor-specific immune responses. *Oncoimmunology*. (2013) 2:e24520. doi: 10.4161/onci.24520
45. Bellone M, Caputo S. Crosstalk between prostate cancer stem cells and immune cells: implications for tumor progression and resistance to immunotherapy. In: Maccalli C, Todaro M, Ferrone S, editors. *Cancer Stem Cell Resistance to Targeted Therapy*. Cham: Springer International Publishing (2019). p. 173–221. doi: 10.1007/978-3-030-16624-3_8
46. Bellone M, Caputo S, Jachetti E. Immunosuppression via tenascin-C. *Oncoscience*. (2015) 2:667–8. doi: 10.18632/oncoscience.210
47. Pan GJ, Chang ZY, Scholer HR, Pei D. Stem cell pluripotency and transcription factor Oct4. *Cell Res*. (2002) 12:321–9. doi: 10.1038/sj.cr.7290134
48. Sangiolo D, Mesiano G, Gammaitoni L, Leuci V, Todorovic M, Giraudo L, et al. Cytokine-induced killer cells eradicate bone and soft-tissue sarcomas. *Cancer Res*. (2014) 74:119–29. doi: 10.1158/0008-5472.CAN-13-1559
49. Demotte N, Stroobant V, Courtoy PJ, Van Der Smissen P, Colau D, Luescher IF, et al. Restoring the association of the T cell receptor with CD8 reverses anergy in human tumor-infiltrating lymphocytes. *Immunity*. (2008) 28:414–24. doi: 10.1016/j.immuni.2008.01.011
50. Tomlins SA, Mehra R, Rhodes DR, Cao X, Wang L, Dhanasekaran SM, et al. Integrative molecular concept modeling of prostate cancer progression. *Nat Genet*. (2007) 39:41–51. doi: 10.1038/ng1935
51. Fortuna-Costa A, Gomes AM, Kozlowski EO, Stelling MP, Pavao MS. Extracellular galectin-3 in tumor progression and metastasis. *Front Oncol*. (2014) 4:138. doi: 10.3389/fonc.2014.00138
52. Nakajima K, Kho DH, Yanagawa T, Harazono Y, Hogan V, Chen W, et al. Galectin-3 cleavage alters bone remodeling: different outcomes in breast and prostate cancer skeletal metastasis. *Cancer Res*. (2016) 76:1391–402. doi: 10.1158/0008-5472.CAN-15-1793
53. Gelman IH. How the TRAMP model revolutionized the study of prostate cancer progression. *Cancer Res*. (2016) 76:6137–9. doi: 10.1158/0008-5472.CAN-16-2636
54. Siegel RL, Miller KD, Jemal A. Cancer statistics, 2018. *CA Cancer J Clin*. (2018) 68:7–30. doi: 10.3322/caac.21442
55. Halabi S, Kelly WK, Ma H, Zhou H, Solomon NC, Fizazi K, et al. Meta-analysis evaluating the impact of site of metastasis on overall survival in men with castration-resistant prostate cancer. *J Clin Oncol*. (2016) 34:1652–9. doi: 10.1200/JCO.2015.65.7270
56. Kwek SS, Cha E, Fong L. Unmasking the immune recognition of prostate cancer with CTLA4 blockade. *Nat Rev Cancer*. (2012) 12:289–97. doi: 10.1038/nrc3223
57. Rigamonti N, Bellone M. Prostate cancer, tumor immunity and a renewed sense of optimism in immunotherapy. *Cancer Immunol Immunother*. (2012) 61:453–68. doi: 10.1007/s00262-012-1216-6
58. Drake CG, Doody AD, Mihalyo MA, Huang CT, Kelleher E, Ravi S, et al. Androgen ablation mitigates tolerance to a prostate/prostate cancer-restricted antigen. *Cancer Cell*. (2005) 7:239–49. doi: 10.1016/j.ccr.2005.01.027
59. Degl'innocenti E, Grioni M, Capuano G, Jachetti E, Freschi M, Bertilaccio MT, et al. Peripheral T-cell tolerance associated with prostate cancer is independent from CD4+CD25+ regulatory T cells. *Cancer Res*. (2008) 68:292–300. doi: 10.1158/0008-5472.CAN-07-2429
60. Wada S, Yoshimura K, Hipkiss EL, Harris TJ, Yen HR, Goldberg MV, et al. Cyclophosphamide augments antitumor immunity: studies in an autochthonous prostate cancer model. *Cancer Res*. (2009) 69:4309–18. doi: 10.1158/0008-5472.CAN-08-4102
61. Bronte V, Kasic T, Gri G, Gallana K, Borsellino G, Marigo I, et al. Boosting antitumor responses of T lymphocytes infiltrating human prostate cancers. *J Exp Med*. (2005) 201:1257–68. doi: 10.1084/jem.20042028
62. Rigamonti N, Capuano G, Ricupito A, Jachetti E, Grioni M, Generoso L, et al. Modulators of arginine metabolism do not impact on peripheral T-cell tolerance and disease progression in a model of spontaneous prostate cancer. *Clin Cancer Res*. (2011) 17:1012–23. doi: 10.1158/1078-0432.CCR-10-2547
63. Ellerhorst J, Troncoso P, Xu XC, Lee J, Lotan R. Galectin-1 and galectin-3 expression in human prostate tissue and prostate cancer. *Urol Res*. (1999) 27:362–7. doi: 10.1007/s002400050164

64. Ding Z, Wu CJ, Chu GC, Xiao Y, Ho D, Zhang J, et al. SMAD4-dependent barrier constrains prostate cancer growth and metastatic progression. *Nature*. (2011) 470:269–73. doi: 10.1038/nature09677
65. Makarov DV, Humphreys EB, Mangold LA, Carducci MA, Partin AW, Eisenberger MA, et al. The natural history of men treated with deferred androgen deprivation therapy in whom metastatic prostate cancer developed following radical prostatectomy. *J Urol*. (2008) 179:156–61; discussion 161–52. doi: 10.1016/j.juro.2007.08.133
66. Chen HY, Fermin A, Vardhana S, Weng IC, Lo KF, Chang EY, et al. Galectin-3 negatively regulates TCR-mediated CD4+ T-cell activation at the immunological synapse. *Proc Natl Acad Sci USA*. (2009) 106:14496–501. doi: 10.1073/pnas.0903497106
67. Demetriou M, Granovsky M, Quaggin S, Dennis JW. Negative regulation of T-cell activation and autoimmunity by Mgat5 N-glycosylation. *Nature*. (2001) 409:733–9. doi: 10.1038/35055582
68. Lagana A, Goetz JG, Cheung P, Raz A, Dennis JW, Nabi IR. Galectin binding to Mgat5-modified N-glycans regulates fibronectin matrix remodeling in tumor cells. *Mol Cell Biol*. (2006) 26:3181–93. doi: 10.1128/MCB.26.8.3181-3193.2006
69. Probstmeier R, Montag D, Schachner M. Galectin-3, a beta-galactoside-binding animal lectin, binds to neural recognition molecules. *J Neurochem*. (1995) 64:2465–72. doi: 10.1046/j.1471-4159.1995.64062465.x
70. Tews DS. Adhesive and invasive features in gliomas. *Pathol Res Pract*. (2000) 196:701–11. doi: 10.1016/S0344-0338(00)80122-3
71. Califice S, Castronovo V, Bracke M, Van Den Brule F. Dual activities of galectin-3 in human prostate cancer: tumor suppression of nuclear galectin-3 vs tumor promotion of cytoplasmic galectin-3. *Oncogene*. (2004) 23:7527–36. doi: 10.1038/sj.onc.1207997
72. Rabinovich GA, Croci DO. Regulatory circuits mediated by lectin-glycan interactions in autoimmunity and cancer. *Immunity*. (2012) 36:322–35. doi: 10.1016/j.immuni.2012.03.004
73. Stowell SR, Cho M, Feasley CL, Arthur CM, Song X, Colucci JK, et al. Ligand reduces galectin-1 sensitivity to oxidative inactivation by enhancing dimer formation. *J Biol Chem*. (2009) 284:4989–99. doi: 10.1074/jbc.M808925200
74. Yoshii T, Fukumori T, Honjo Y, Inohara H, Kim HR, Raz A. Galectin-3 phosphorylation is required for its anti-apoptotic function and cell cycle arrest. *J Biol Chem*. (2002) 277:6852–7. doi: 10.1074/jbc.M107668200
75. Wdowiak K, Francuz T, Gallego-Colon E, Ruiz-Agamez N, Kubeczko M, Grochola I, et al. Galectin targeted therapy in oncology: current knowledge and perspectives. *Int J Mol Sci*. (2018) 19:210. doi: 10.3390/ijms19010210
76. Streetly MJ, Maharaj L, Joel S, Schey SA, Gribben JG, Cotter FE. GCS-100, a novel galectin-3 antagonist, modulates MCL-1, NOXA, and cell cycle to induce myeloma cell death. *Blood*. (2010) 115:3939–48. doi: 10.1182/blood-2009-10-251660
77. Yan J, Katz A. PectaSol-C modified citrus pectin induces apoptosis and inhibition of proliferation in human and mouse androgen-dependent and-independent prostate cancer cells. *Integr Cancer Ther*. (2010) 9:197–203. doi: 10.1177/1534735410369672
78. Hossein G, Halvaei S, Heidarian Y, Dehghani-Ghobadi Z, Hassani M, Hosseini H, et al. Pectasol-C modified citrus pectin targets galectin-3-induced STAT3 activation and synergize paclitaxel cytotoxic effect on ovarian cancer spheroids. *Cancer Med*. (2019) 8:4315–29. doi: 10.1002/cam4.2334
79. Demotte N, Wieers G, Van Der Smissen P, Moser M, Schmidt C, Thielemans K, et al. A galectin-3 ligand corrects the impaired function of human CD4 and CD8 tumor-infiltrating lymphocytes and favors tumor rejection in mice. *Cancer Res*. (2010) 70:7476–88. doi: 10.1158/0008-5472.CAN-10-0761
80. Guha P, Kaptan E, Bandyopadhyaya G, Kaczanowska S, Davila E, Thompson K, et al. Cod glycopeptide with picomolar affinity to galectin-3 suppresses T-cell apoptosis and prostate cancer metastasis. *Proc Natl Acad Sci USA*. (2013) 110:5052–7. doi: 10.1073/pnas.1202653110
81. Farhad M, Rolig AS, Redmond WL. The role of galectin-3 in modulating tumor growth and immunosuppression within the tumor microenvironment. *Oncoimmunology*. (2018) 7:e1434467. doi: 10.1080/2162402X.2018.1434467
82. Elia AR, Caputo S, Bellone M. Immune checkpoint-mediated interactions between cancer and immune cells in prostate adenocarcinoma and melanoma. *Front Immunol*. (2018) 9:1786. doi: 10.3389/fimmu.2018.01786

Conflict of Interest: The authors declare that the research was conducted in the absence of any commercial or financial relationships that could be construed as a potential conflict of interest.